

Article

Effects of Trace Si Addition on the Microstructures and Tensile Properties of Ti-3Al-8V-6Cr-4Mo-4Zr Alloy

Hongbo Ba, Limin Dong *, Zhiqiang Zhang and Xiaofei Lei

Institute of Metal Research, Chinese Academy of Sciences, 72 Wenhua Road, Shenyang 110016, China; bahongbo@sina.com (H.B.); zqzhang@imr.ac.cn (Z.Z.); xfle13b@imr.ac.cn (X.L.)

* Correspondence: lmdong@imr.ac.cn; Tel.: +86-242-397-1942

Received: 16 June 2017; Accepted: 24 July 2017; Published: 27 July 2017

Abstract: The microstructural evolution and tensile properties of Ti-3Al-8V-6Cr-4Mo-4Zr titanium alloys with various Si contents were investigated. The results revealed that the addition of trace Si and the presence of Zr induced the formation of $(\text{TiZr})_6\text{Si}_3$ silicides, in the size range from 100 nm to 300 nm. The fine silicide precipitates refined β grains. The tensile strength increased about 40 MPa due to precipitation strengthening and grain refinement, and the ductility of the two alloys was similar. The tensile fracture mode of the alloys was dimple ductile fracture.

Keywords: titanium alloy; microstructure; silicide; tensile properties

1. Introduction

Titanium alloys are widely used in aerospace applications due to their high strength to weight ratio and excellent corrosion resistance [1–3]. Except for compressor disks and blades, a considerable fraction of fasteners and springs are fabricated from $\alpha + \beta$ and β titanium alloys, because they exhibit a favorable strength/toughness combination and high fatigue strength [4,5]. Among these titanium alloys, the β type Ti-3Al-8V-6Cr-4Mo-4Zr (known as Beta C) alloy has attracted the attention of researchers in recent years [6,7]. This alloy is developed from Ti-13V-11Cr-3Al, and it is easier to melt and exhibits less segregation due to a low Cr content [8]. In addition, the alloy can be hardened by solution plus aging treatment, and its ultimate tensile strength can reach 1380 MPa [8,9]. It can be utilized in either solution-treated or solution-aging-treated conditions; thus, a wide variation in mechanical properties can be obtained for different applications. However, the rapid β grain coarsening is still an open problem when they are solution-treated above the β transus, especially for β type titanium alloys.

The changes in microstructures and phase structures influence the mechanical properties of titanium alloys significantly. For β type titanium alloys, the body-centered cubic β phases possess good ductility, and precipitated α phases enhance their strength after aging treatment. For high-temperature titanium alloys, such as Ti-5.8Al-4Sn-3.5Zr-0.7Nb-0.35Si-0.06C [10] or Ti-6.3Al-1.6Zr-3.4Mo-0.3Si [11], the addition of Si can improve their creep performances due to the precipitation of silicides. Up to now, two different types of Ti-Zr-Si ternary silicides have been recognized in titanium alloys, S1 ($a = 0.780$ nm, $c = 0.544$ nm) and S2 ($a = 0.701$ nm, $c = 0.368$ nm), with stoichiometries $(\text{TiZr})_5\text{Si}_3$ and $(\text{TiZr})_6\text{Si}_3$ [12–14], respectively. Flower et al. [15] reported that they have a hexagonal crystal structure in aged Ti-5Zr-1Si alloy, using X-ray diffraction.

Apart from improving the creep properties, the addition of Si also plays an important role in inhibiting β grain growth. Bermingham et al. [16] showed that a small amount of Si addition to commercial purity Ti produced fine prior- β grains. Tavares et al. [17] presented that the Si addition to the β type Ti-35Nb alloy made beta phases more stable and achieved grain refinement. However, the addition of high amounts of Si

will decrease the ductility of titanium alloys at room temperature. Ramachandra and Singh [18,19] showed that the presence of 0.25 wt % Si in Ti-6Al-5Zr-0.5Mo-0.25Si alloy led to a drastic reduction in tensile ductility at room temperature. In terms of Ti-3Al-8V-6Cr-4Mo-4Zr alloy, Morito et al. [20] also investigated the effect of higher than 0.2 wt % Si addition on the microstructure and aging behavior, but high contents of Si was found to possibly embrittle this alloy. In order to obtain the balance of strength and ductility for industrial applications, it is necessary to gain more insight into the effect of trace Si addition on the microstructures and properties of Ti-3Al-8V-6Cr-4Mo-4Zr alloy.

Based on the above, trace Si as an alloying element was added to Ti-3Al-8V-6Cr-4Mo-4Zr alloy, and the objective of the experiment was to investigate the influence of Si either in solution or in the form of silicides on its microstructures and performances.

2. Materials and Methods

In this study, Ti-3Al-8V-6Cr-4Mo-4Zr (designated C1) and Ti-3Al-8V-6Cr-4Mo-4Zr-0.05Si (designated C2) alloys were fabricated from pure Ti, Al, V, Cr, Mo, Zr and Si ($\geq 99.9\%$ purity) by three times vacuum arc melting and conventional rolling. The chemical compositions of the two alloys are listed in Table 1. The β transus for the alloys was ~ 740 °C, as measured by a metallographic technique. The rolled bars, 12 mm in diameter, for both alloys were cut and subjected to solution treatment at 800 °C for 1 h, and were then water quenched to room temperature.

Table 1. Chemical composition of the alloys.

Alloy	Composition (wt %)						
	Al	V	Cr	Mo	Zr	Si	Ti
C1	3.54	8.00	6.02	4.05	4.00	0.02	Bal.
C2	3.48	8.00	5.95	4.05	4.00	0.06	Bal.

The microstructures were characterized using an optical microscope (OM, ZEISS Axiovert 200MAT, Carl Zeiss Shanghai Co., Ltd, Shanghai, China) and scanning electron microscope (SEM, ShimadzuSSX-550, Shimadzu Corporation, Tokyo, Japan) equipped with an Energy Dispersive X-ray (EDX) detector, after samples were manually grounded, polished and chemically etched for 30 s in a solution of 5% HF, 10% HNO₃, and 85% water at room temperature. The back-scattered electron (BSE) mode was utilized for the observation of precipitates, and the polished samples were not be etched to avoid the dissolution of silicides into the HF etchant. Image-Pro Plus software was utilized for grain size analysis, and the grain size distributions were obtained. The average grain size and standard deviation were calculated on the basis of the grain diameter. TEM specimens were manually ground down to a thickness of 50 μm , punched into discs of Φ 3 mm, and then ion-milled to electron transparency in a Gatan ion miller. TEM observation was performed on a Tecnai G2 20 transmission electron microscope (TEM) (FEI Company, Hillsboro, OR, USA) with an Energy Dispersive Spectroscopy (EDS).

Tensile tests at room temperature were carried out on an Instron 5582 testing machine (Instron, Chicago, IL, USA) at a constant cross-head speed of 1 mm/min. Two specimens were tested for each alloy. Tensile specimens with a gage diameter of 5 mm and a gage length of 30 mm were used. The fracture morphologies were observed by SEM.

3. Results and Discussion

3.1. Microstructure Characteristics

Figure 1 presents the optical microstructures of the alloys after solution treatment at 800 °C for 1 h. The microstructures were composed of equi-axed β grains, and the grain size of alloy C2 was finer than that of alloy C1. The grain size distribution histograms, average grain size, and standard

deviation of both alloys are shown in Figure 2. It can be observed that the grain size distribution is markedly different for the two alloys. In C1, the average grain size was 58 μm , the grain size ranged from 10 μm to 140 μm , and over 44% of the grains were larger than 60 μm . In C2, the average grain size was 31 μm , and almost all grains were in the grain size range between 10 μm and 60 μm . The standard deviation of the alloys was 25 μm and 9 μm , respectively. These results indicate that the grain size uniformity of alloy C2 is superior to that of C1.

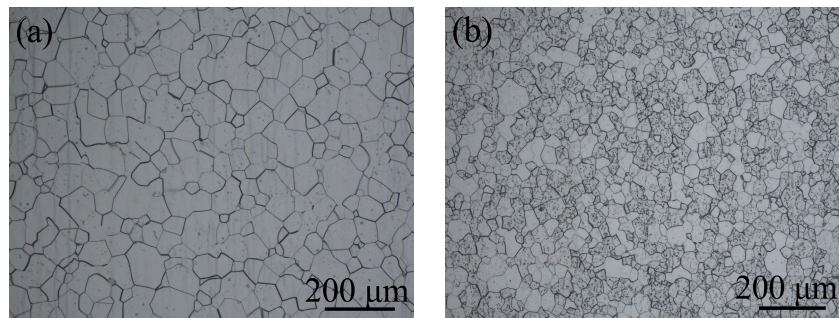


Figure 1. Optical microstructures of the alloys after solution treatment at 800 °C for 1 h: (a) alloy C1; (b) alloy C2.

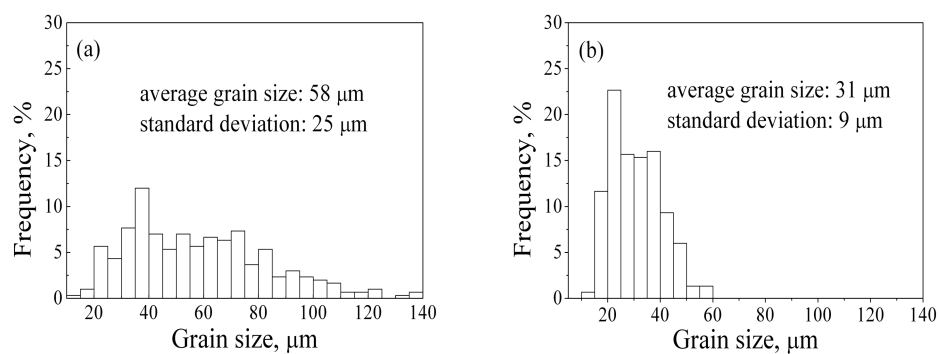


Figure 2. Grain size distributions of alloys: (a) alloy C1; (b) alloy C2.

Figure 3 shows the BSE images and EDX spectra of the alloys in solution-treated condition before etching. No resolvable precipitates are observed in C1 (Figure 3a), while white particles are clearly observed in C2 (Figure 3b). Although the distribution and morphologies of particles are not exactly confirmed in polished C2 samples, the size is very tiny. By comparison, no Si peak is found in the EDX spectra for the matrix (Figure 3c), but the white precipitates are rich in Zr and Si (Figure 3d). This confirms that the white particles are Ti-Zr-Si silicides.

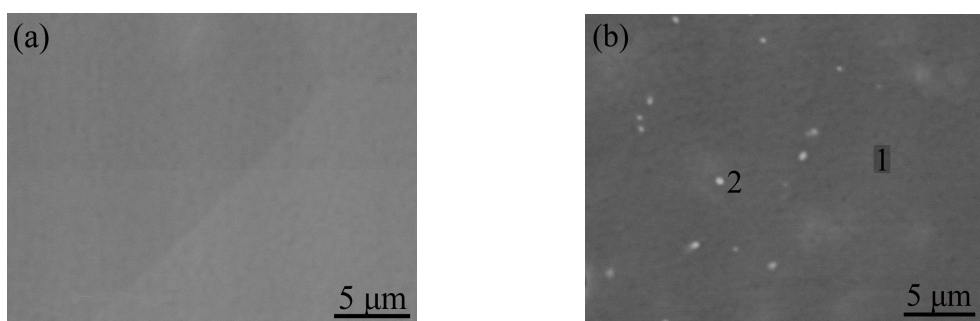


Figure 3. Cont.

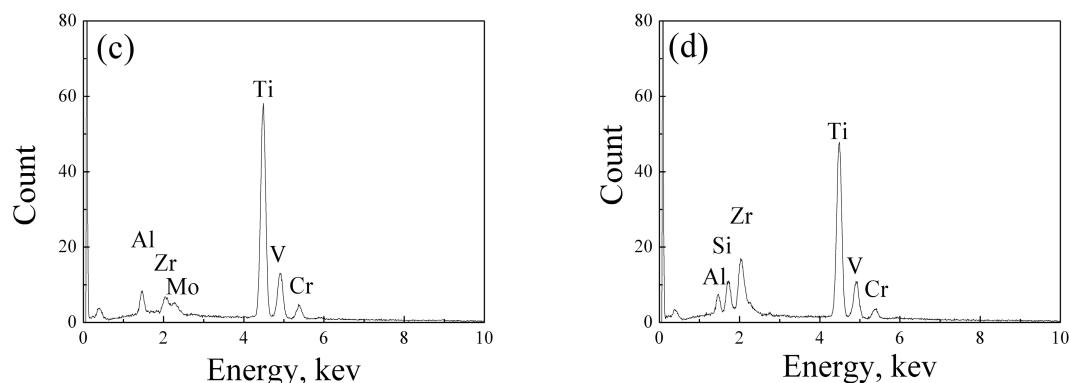


Figure 3. BSE (Back-Scattered Electron) images of microstructures of C1 (a) and C2 (b) before etching; EDX (Energy Dispersive X-ray) spectra of matrix marked by 1 (c) and white precipitates marked by 2 (d).

The selected area electron diffraction (SAED) and EDS analysis were carried out on TEM, and the precipitate was particle shaped, about 200 nm in size (Figure 4a). The precipitate is rich in Zr and Si, identified as the $(\text{TiZr})_6\text{Si}_3$ silicides through the electron diffraction pattern (Figure 4b) and composition information (Figure 4c,d).

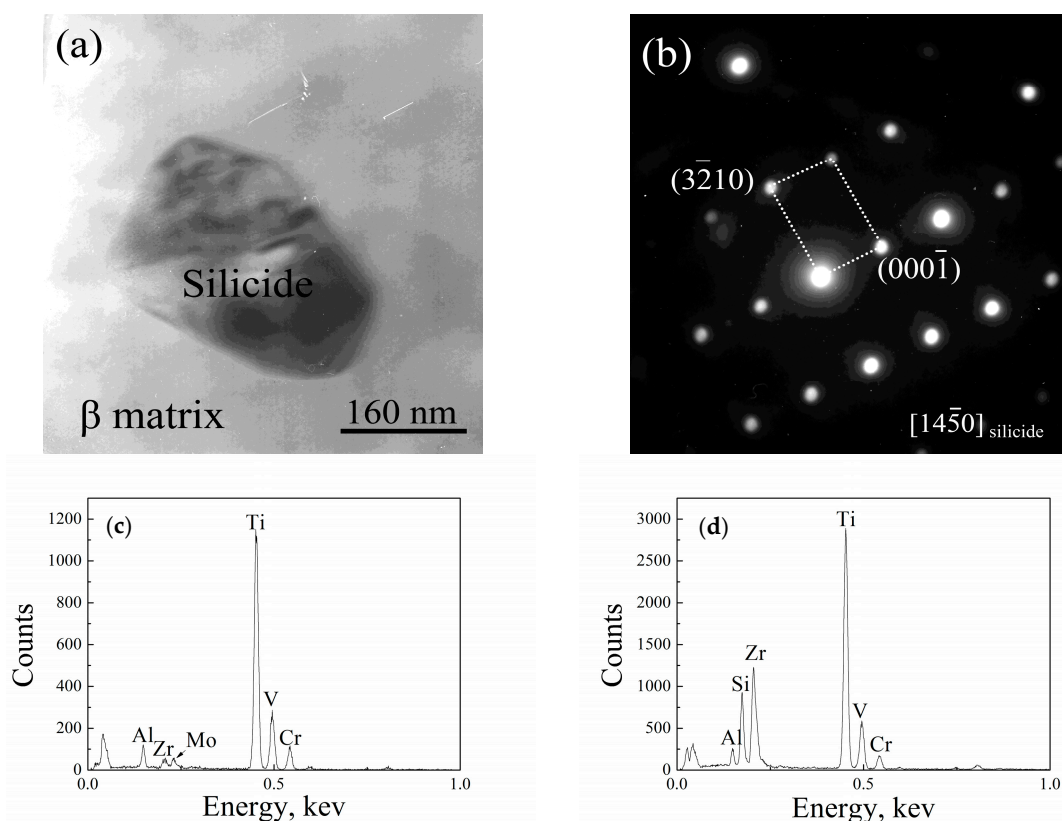


Figure 4. TEM image (a); corresponding SAED (Selected Area Electron Diffraction) pattern for the silicide (b); EDS (Energy Dispersive Spectroscopy) spectra of β matrix (c) and silicide (d) for solution-treated alloy C2.

Earlier studies demonstrated that Zr addition will promote the formation of silicides in titanium alloys [11,12,21]. Therefore, the precipitation of silicides resulted from the addition of Si and the presence of Zr in alloy C2. However, the Si content in C1 is only ~ 0.02 wt % from raw materials, which is below the saturation concentration of Si in the alloy, therefore Si dissolves in the β matrix.

Figure 5 shows the SEM morphologies of microstructures of both alloys after etching. There are no etch pits in C1, but a large number of etch pits are observed in alloy C2, marked by the arrow. It is a common chemical phenomenon that silicides are dissolved by the HF etchant, hence the formation of etch pits should result from the dissolution of silicides. Meanwhile, it is reasonable that the quantity and sites of etch pits correspond to those of silicides in alloy C2. According to the distribution of etch pits, it is deduced that silicides precipitate both on the β grain boundaries and in the interior of grains (Figure 5b).

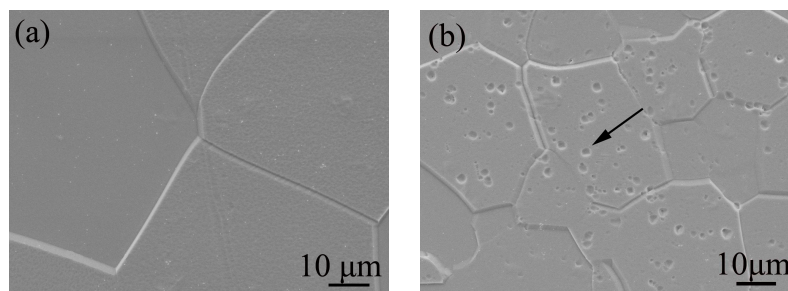


Figure 5. SEM morphologies of microstructures of the alloys after etching: (a) alloy C1; (b) alloy C2.

Singh et al. [22] reported that the kinetics of silicide precipitation in Ti-6Al-1.6Zr-3.3Mo-0.3Si (VT9) alloy was faster than in Ti-6Al-5Zr-0.5Mo-0.25Si (IMI685), which was attributed to the higher content of strong β -stabilizing element Mo in the former alloy. Therefore, it is understandable that the kinetics of the precipitation of silicides is fast in C2. On one hand, fine dispersed silicide precipitates promote the recrystallization nuclei during solution treatment at 800 °C. On the other hand, fine silicides play an important role in hindering the movement of the grain boundaries during the grain growth. This is the reason why alloy C2 has a much finer grain size.

3.2. Tensile Properties

The tensile stress-strain curves of both alloys are presented in Figure 6. A summary of the data is given in Table 2. Based on these data, it can be seen that the yield strength (YS) and ultimate tensile strength (UTS) of alloy C2 are about 40 MPa higher than those of C1, respectively. Meanwhile, there is a slight decrease in the elongation (El) and the reduction in area (RA). These results are similar to those found in the literature [23–25], where the silicide precipitates are considered to lead to an increase in strength and a slight drop in ductility for near α titanium alloys.

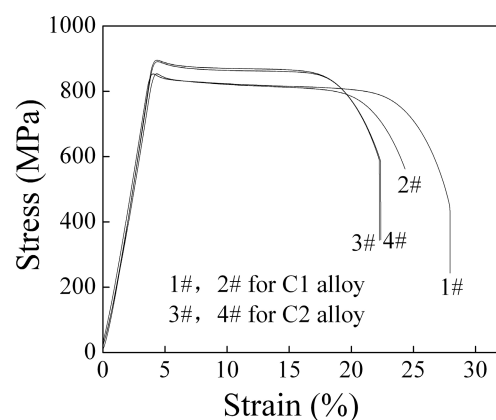


Figure 6. Tensile stress-strain curves of C1 and C2 alloys solution-treated at 800 °C for 1 h.

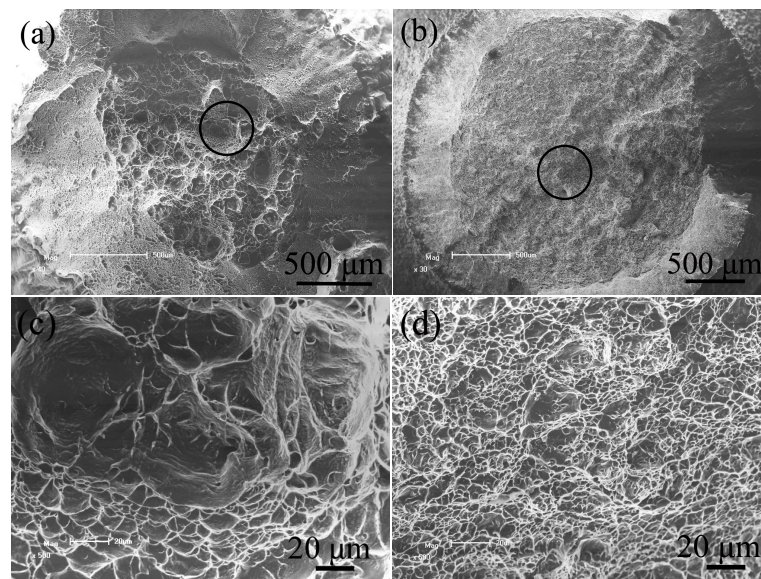
Table 2. Tensile properties of both alloys solution treated at 800 °C for 1 h.

Alloy	YS, MPa	UTS, MPa	El, %	RA, %
C1	852	853	29.0	73
	852	854	27.5	76
C2	888	891	23.5	62
	893	896	24.0	61

The differences in the tensile properties of the alloys are largely due to their microstructures. Firstly, the β grain size of alloy C2 was finer than that of C1. According to the Hall-Petch law, grain refinement enhances yield strength [26,27]. Secondly, a large number of fine silicides dispersed in alloy C2, which have an effect of precipitation strengthening. These explain the difference in the tensile properties of the alloys.

The changes in ductility also result from the precipitation of dispersed silicides, which would hinder the dislocation motion during tensile deformation. The precipitates tend to induce local stress concentration and crack initiation, resulting in the slightly low plasticity of alloy C2.

Figure 7 shows the fracture morphologies of both alloys. The fracture consists of fibrous and shear lip zones (Figure 7a,b). A large number of dimples spread across the fracture surfaces, which are the characteristic of ductile fracture. Dimples are more uniform and smaller in alloy C2 than those in C1 (Figure 7c,d). This is related to the presence of the dispersed silicides in alloy C2. Compared with C2, alloy C1 experiences a larger plastic deformation before fracture, resulting from its single β phase microstructure.

**Figure 7.** Tensile fractographies of the alloys: (a,c): alloy C1; (b,d): alloy C2.

4. Conclusions

- (1) The addition of trace amount of Si (~0.05 wt %) and the presence of 4 wt % Zr induced the formation of $(\text{TiZr})_6\text{Si}_3$ silicides in Ti-3Al-8V-6Cr-4Mo-4Zr-0.05Si alloy.
- (2) The dispersed silicides refined β grains, and the average grain size of Ti-3Al-8V-6Cr-4Mo-4Zr-0.05Si alloy was more uniform than that of Ti-3Al-8V-6Cr-4Mo-4Zr alloy. Adding Si was an effective way to refine β grains for the Ti-3Al-8V-6Cr-4Mo-4Zr alloy.

- (3) The silicide precipitates enhanced the tensile strength of Ti-3Al-8V-6Cr-4Mo-4Zr-0.05Si alloy, and the change in ductility was slight. The increase in strength was attributed to both precipitation strengthening and grain refinement. The fracture mode of both alloys was ductile.

Author Contributions: Hongbo Ba and Limin Dong conceived and designed the experiments; Hongbo Ba, Zhiqiang Zhang, and Xiaofei Lei performed the experiments and analyzed the data; Hongbo Ba wrote the paper.

Conflicts of Interest: The authors declare no conflict of interest.

References

1. Williams, J.C.; Starke, E.A. Progress in structural materials or aerospace systems. *Acta Mater.* **2003**, *51*, 5775–5799. [[CrossRef](#)]
2. Banerjee, D.; Williams, J.C. Perspectives on titanium science and technology. *Acta Mater.* **2013**, *61*, 844–879. [[CrossRef](#)]
3. Lei, X.F.; Dong, L.M.; Zhang, Z.Q.; Liu, Y.J.; Hao, Y.L.; Yang, R.; Zhang, L.C. Microstructure, texture evolution and mechanical properties of VT3-1 titanium alloy processed by multi-pass drawing and subsequent isothermal annealing. *Metals* **2017**, *7*, 131. [[CrossRef](#)]
4. Kim, J.H.; Lee, C.H.; Hong, J.K.; Kim, J.H.; Yeom, J.T. Effect of surface treatment on the hot forming of the high strength Ti-6Al-4V fastener. *Mater. Trans.* **2009**, *50*, 2050–2056. [[CrossRef](#)]
5. Kume, K.; Furui, M.; Ikeno, S.; Ishisaka, Y.; Yamamoto, M. Screw form rolling of beta type titanium alloy preliminary worked by torsion. *Mater. Sci. Forum* **2010**, *654*, 906–909. [[CrossRef](#)]
6. Solek, A.L.; Krawczyk, J. The analysis of the hot deformation behaviour of the Ti-3Al-8V-6Cr-4Zr-4Mo alloy, using processing maps, a map of microstructure and of hardness. *Mater. Des.* **2015**, *65*, 165–173. [[CrossRef](#)]
7. Salam, A.; Hammond, C. Superplasticity and associated activation energy in Ti-3Al-8V-6Cr-4Mo-4Zr alloy. *J. Mater. Sci.* **2005**, *40*, 5475–5482. [[CrossRef](#)]
8. Boyer, R.; Welsch, G.; Collings, E.W. *Materials Properties Handbook: Titanium Alloys*, 1st ed.; ASM International: Materials Park, OH, USA, 1994; pp. 797–828.
9. Schmidt, P.; El-chaikl, A.; Christ, H.J. Effect of duplex aging on the initiation and propagation of fatigue cracks in the solute-rich metastable β titanium alloy Ti 38–644. *Metall. Mater. Trans. A* **2011**, *42*, 2652–2667. [[CrossRef](#)]
10. Es-souni, M. Creep behaviour and creep microstructures of a high-temperature titanium alloy Ti-5.8Al-4.0Sn-3.5Zr-0.7Nb-0.35Si-0.06C (Timetal 834): Part I. Primary and steady-state creep. *Mater. Charact.* **2001**, *46*, 365–379. [[CrossRef](#)]
11. Gu, Y.; Zeng, F.H.; Qi, Y.L.; Xia, X.Q.; Xiong, X. Tensile creep behavior of heat-treated TC11 titanium alloy at 450–550 °C. *Mater. Sci. Eng. A* **2013**, *575*, 74–85. [[CrossRef](#)]
12. Singh, A.K.; Ramachandra, C. Characterization of silicides in high-temperature titanium alloys. *J. Mater. Sci.* **1996**, *32*, 229–234. [[CrossRef](#)]
13. Li, J.X.; Wang, L.Q.; Qin, J.N.; Chen, Y.F.; Lu, W.J.; Zhang, D. The effect of heat treatment on thermal stability of Ti matrix composite. *J. Alloys Compd.* **2011**, *509*, 52–56. [[CrossRef](#)]
14. Ramachandra, C.; Singh, V. Silicide precipitation in alloy Ti-6Al-5Zr-0.5Mo-0.25Si. *Metall. Trans. A* **1982**, *13*, 771–775. [[CrossRef](#)]
15. Flower, H.M.; Swann, P.R.; West, D.R.F. Silicide precipitation in the Ti-Zr-Al-Si system. *Metall. Mater. Trans. B* **1971**, *2*, 3289–3297. [[CrossRef](#)]
16. Bermingham, M.J.; McDonald, S.D.; Dargusch, M.S.; Stjohn, D.H. The mechanism of grain refinement of titanium by silicon. *Scr. Mater.* **2008**, *58*, 1050–1053. [[CrossRef](#)]
17. Tavares, A.M.G.; Ramos, W.S.; Blas, J.C.G.; Lopes, E.S.N.; Caram, R.; Batista, W.W.; Souza, S.A. Influence of Si addition on the microstructure and mechanical properties of Ti-35Nb alloy for applications in orthopedic implants. *J. Mech. Behav. Biomed. Mater.* **2015**, *51*, 74–87. [[CrossRef](#)] [[PubMed](#)]
18. Ramachandra, C.; Singh, V. Effect of silicide precipitation on tensile properties and fracture of alloy Ti-6Al-5Zr-0.5Mo-0.25Si. *Metall. Trans. A* **1985**, *16*, 227–231. [[CrossRef](#)]
19. Ramachandra, C.; Singh, V. Effect of silicides on tensile properties and fracture of alloy Ti-6Al-5Zr-0.5Mo-0.25Si from 300 to 823 K. *J. Mater. Sci.* **1988**, *23*, 835–841. [[CrossRef](#)]

20. Morito, F.; Muneki, S.; Takahashi, J.; Kainuma, T. The effect of Silicon Addition on the Microstructure and the Aging Behavior of Ti-3Al-8V-6Cr-4Mo-4Zr Alloy. In Proceedings of the Titanium 95: Eighth World Congress on Titanium, Birmingham, UK, 22–26 October 1995; pp. 2494–2501.
21. Singh, A.K.; Roy, T.; Ramachandra, C. Microstructural stability on aging of an $\alpha + \beta$ titanium alloy: Ti-6Al-1.6Zr-3.3Mo-0.30Si. *Metall. Mater. Trans. A* **1996**, *27*, 1167–1173. [[CrossRef](#)]
22. Singh, A.K.; Ramachandra, C.; Tavafoghi, M.; Singh, V. Microstructure of β -solution-treated, quenched and aged $\alpha + \beta$ titanium alloy Ti-6Al-1.6Zr-3.3Mo-0.30Si. *J. Alloys Compd.* **1992**, *179*, 125–135. [[CrossRef](#)]
23. Jayaprakash, M.; Ping, K.H.; Yamabe-mttaeai, Y. Effect of Zr and Si addition on high temperature mechanical properties of near- α Ti-Al-Zr-Sn based alloys. *Mater. Sci. Eng. A* **2014**, *612*, 456–461. [[CrossRef](#)]
24. Popov, A.; Rossina, N.; Popova, M. The effect of alloying on the ordering processes in near-alpha titanium alloys. *Mater. Sci. Eng. A* **2013**, *564*, 284–287. [[CrossRef](#)]
25. Jia, W.; Zeng, W.; Yu, H. Effect of aging on the tensile properties and microstructures of a near-alpha titanium alloy. *Mater. Des.* **2014**, *58*, 108–115. [[CrossRef](#)]
26. Tsai, Y.L.; Wang, S.F.; Bor, H.Y.; Hsu, Y.F. Effects of Zr addition on the microstructure and mechanical behavior of a fine-grained nickel superalloy at elevated temperatures. *Mater. Sci. Eng. A* **2014**, *607*, 294–301. [[CrossRef](#)]
27. Muszka, K.; Majta, J.; Bienias, L. Effect of grain refinement on mechanical properties of microalloyed steels. *Metall. Found. Eng.* **2006**, *32*, 87–97. [[CrossRef](#)]



© 2017 by the authors. Licensee MDPI, Basel, Switzerland. This article is an open access article distributed under the terms and conditions of the Creative Commons Attribution (CC BY) license (<http://creativecommons.org/licenses/by/4.0/>).